

# A Conceptual Design Study of a Compact Photon Source (CPS) for Jefferson Lab

E. Chudakov,<sup>1</sup> D. Day,<sup>2</sup> P. Degtiarenko,<sup>1</sup> R. Ent,<sup>1</sup> D.J. Hamilton,<sup>3</sup>  
T. Horn,<sup>4,1,\*</sup> D. Keller,<sup>2</sup> C. Keppel,<sup>1</sup> G. Niculescu,<sup>5</sup>  
P. Reid,<sup>6</sup> I. Strakovsky,<sup>7</sup> B. Wojtsekhowski,<sup>1</sup> and J. Zhang<sup>2</sup>

<sup>1</sup>*Jefferson Lab*

<sup>2</sup>*University of Virginia*

<sup>3</sup>*University of Glasgow*

<sup>4</sup>*Catholic University of America*

<sup>5</sup>*James Madison University*

<sup>6</sup>*Saint Mary's University*

<sup>7</sup>*George Washington University*

---

\* Contact email: [hornt@cua.edu](mailto:hornt@cua.edu)

# I Executive Summary

This document describes the technical design concept of a compact, high intensity photon source (CPS) to be used with dynamically nuclear polarized targets to measure processes such as Wide-Angle and Timelike Compton Scattering (WACS and TCS). Capable of producing  $10^{12}$  equivalent photons per second, the deployment of the CPS will result in a large gain in polarized experiment figure-of-merit (by a factor of  $\sim 30$ ). Compared to a traditional bremsstrahlung photon source the proposed solution will present several advantages, including much lower radiation levels, both prompt and post-operational due to the beam line elements radio-activation. For use with polarized targets, the heat load and radiation damage effects are well within the acceptable range. The design is flexible allowing the CPS to be converted into a  $K_L$  beam for spectroscopy experiments. PAC43-PAC45 at Jefferson Lab saw several proposals and LOIs which require the CPS. One of these is C12-17-008 (Polarization observables in Wide-angle Compton scattering at large  $s$ ,  $t$ , and  $u$ ), which was conditionally approved subject to a technical review. The issues in the PAC45 report to be addressed are: to finalize the design and price estimate for the CPS, and to clearly establish the expected maximum photon intensity. **The goal of this document is to address the PAC45 technical comments for full approval of C12-17-008.**

The CPS final design features a magnet, a central copper absorber, and hermetic shielding consisting of tungsten powder and borated plastic. The addition of the latter has a considerable impact on reducing the neutron flux escaping the CPS. The ultimate goal in this design process is that radiation from the source should be a few times less than from a photon beam interacting with the material of a polarized target. The equivalent heat load for a pure photon beam impinging such targets corresponds to a photon flux originating from a  $2.7 \mu\text{A}$  electron beam current striking a 10% Cu radiator. Detailed simulations of the power density and heat flow analysis show that the maximum temperature in the absorber is below 400 degrees, which is well within the acceptable range of copper, and thus demonstrates that the CPS can absorb 30 kW in total (corresponding to 11 GeV beam energy and  $2.7 \mu\text{A}$  beam current).

The CPS fulfills the requirements on operational dose rates at Jefferson Lab, which has been established with extensive and realistic simulations. The projected prompt dose rate at the site boundary is less than  $1 \mu\text{rem/hr}$  (to be compared with  $2.4 \mu\text{rem/hr}$ , which corresponds to a typical JLab experiment that does not require extra shielding). The activation dose outside the device envelope at one foot distance is less than several mrem/hr after one hour following the end of a 1000 hour run ( $\sim 40$  PAC days). The activation dose at the pivot in the experimental target area, where operational maintenance tasks may be required, is dominated by the dose induced by the pure photon beam. At a distance of one foot from the scattering chamber it is less than several mrem/hr one hour after the end of a 1000 hour run (i.e. the additional activation dose induced by absorption of the electron beam in the Compact Photon Source is negligible).

**This document demonstrates that the CPS with an optimized shielding design provides a photon flux of  $1.5 \times 10^{12}$  equivalent photons/s, with a factor of 1000 reduction in prompt radiation dose compared to a  $2.7 \mu\text{A}$  (30 kW) electron beam current striking a 10% Cu radiator. The CPS meets the acceptable radiation level requirements for a typical run time of 1000 hours with**

the photon source located at 2-3m from the target. The technical design and installation in the existing hall infrastructure is feasible. The estimated cost is on the order of \$4M and is dominated by the raw material costs of tungsten.

This document is organized as follows. In section II, we outline the science gain with CPS in combination with dynamically nuclear polarized targets including the use of an effective rastering of the beam at these high intensities. The heat load and power deposition are also discussed. In section III, the conceptual design and component details of the CPS are presented. Section IV lists the requirements a CPS has to meet to fulfill operational dose rates at Jefferson Lab. In section V, we discuss the results of our shielding design and optimization studies and compare them with the requirements in section IV. Finally, section VI deals with engineering and safety aspects including material considerations, installation, and a preliminary cost analysis. Appendix 1 describes the CPS concept transfer to Hall D. Appendix 2 includes a benchmark comparison of the different simulations used in our shielding design studies.

## II Motivation: Science Gain with CPS

### A Polarization Observables in Wide-Angle Compton Scattering

Investigating the three-dimensional structure of the nucleon has been an active and productive field of research, especially during the last two decades since the invention of the GPD formalism, and continues to be central to the hadron physics program at JLab. The GPD formalism provides a unified description of several important reactions such as elastic electron scattering, DIS, DVCS/TCS, WACS and meson production, which can all be described by a single set of four functions  $H$ ,  $\tilde{H}$ ,  $E$  and  $\tilde{E}$ . These functions need to be modeled and constrained with parameters extracted from experimental data.

The WACS experimental observables provide several constraints for GPDs which are complementary to other exclusive reactions due to an  $e_a^2$  factor and an additional  $1/x$  weighting in the GPD integrals for WACS. For example, the elastic form factor  $F_1(t) = \sum_a e_a \int dx H^a(x, 0, t)$  is related to the WACS vector form factor  $R_V(t) = \sum_a e_a^2 \int \frac{dx}{x} H^a(x, 0, t)$ , both of which are based on the same underlying GPD  $H(x, 0, t)$ . Similarly, polarized observables in WACS uniquely provide high  $-t$  constraints on  $\tilde{H}(x, \xi, t)$  via extraction of the WACS axial form factor  $R_A(t)$  in a kinematic regime where precise data on the nucleon axial form factor is not available.

Polarized WACS experiments need to be performed at large photon energy and scattering angle where the assumption of a factorized reaction amplitude is valid and the GPD-based calculations are reliable ( $s, |t|, |u| > 2.5 \text{ GeV}^2$ ). The experimental challenges associated with double-polarization measurements of photon-induced reactions at high momentum transfer are formidable. Detector rate capabilities and radiation hardness are both severely tested in beam-recoil measurements as a result of a rapid decrease in recoil proton polarimeter analyzing power at high  $-t$ . Utilization of a mixed electron-photon bremsstrahlung beam, on the other hand, limits luminosity in beam-target measurements due to loss of target polarization, primarily as a result of electron-induced heat load. In

the preparation of a 12 GeV Jefferson Lab experimental proposal (C12-17-008) on polarized wide-angle Compton Scattering (WACS), a completely new experimental approach was developed, based on deploying a high-intensity compact photon beam source and a polarized target. This new technique opens up physics possibilities that had hitherto been inaccessible at tagged photon facilities and results in a significantly improved figure-of-merit (of a factor of  $\sim 30$ ) over all previous double-polarization measurements involving photon-induced reactions.

## B Compatibility with Polarized Targets

### 1 Target System and Required Modifications

The WACS experiment will use a polarized proton target developed by UVa/JLab, which has typically been exposed to a beam of 100 nA electrons and provided a run-averaged proton polarization of approximately 70%. The beam must be moved over the 25 mm face of the target cup to ensure that the target material is exposed uniformly to the depolarizing effects of the beam. If the beam were to remain at one location for an extended period it would drill a 'hole' in the target where the polarization has fallen due to local heating and radiation damage. As the NMR system samples the entire target it would, in this case, indicate a much larger value than that where the scattering was taking place. Rastering the beam across the face of the target continuously removes this problem and was made possible in the past by the combination of the standard hall fast raster of  $\pm 2$  mm and a specially constructed slow raster. However, the CPS presented in this document has a very small exit aperture of 3 mm by 3 mm, limiting possible beam motion.

An alternative approach for the beam-target raster is found in Ref. [1] and includes a combination of the target rotation around the horizontal axis and  $\pm 10$  mm vertical motion of the target ladder. Such a raster method effectively moves the motion complexity out of the high radiation area of the absorber. Here we layout the requirements for the rotation and vertical motion which will provide the same uniform exposure as the electron beam raster system used up to now. We start from the premise that the Compact Photon Source (CPS) target system will be able to handle the the same heat load from the photon beam and the microwaves source as used in electron beam experiments. From the perspective of the low energy production of free radicals in the target material, this approximation is expected to be good within 10%. However the free radical complex produced from a high energy beam ( $E_{beam} > 20$  MeV) and the way these radicals can effect the polarization is not yet well understood. For now we focus only on the ionization energy loss produced by the multi-GeV photon beam as  $e^+/e^-$  pairs. The energy loss from these processes is approximately independent of beam energy and is estimated to be about  $2 \text{ MeV g}^{-1} \text{ cm}^2$ .

For a photon intensity of  $1.5 \times 10^{12}$  equivalent photons per second it is necessary to use an evaporation refrigerator with  $\sim 1$  Watt cooling power in combination with a high polarization, high radiation resistant proton target material ( $\text{NH}_3$ ). For electron beam experiments typically 100 nA is the maximum current on the target. The heat load in a

3 cm long target can be calculated for  $\text{NH}_3$  with density  $0.917 \text{ g/cm}^3$  leading to,

$$2[\text{MeVcm}^2/\text{g}](1.6 \times 10^{-13}[\text{J/MeV}])6.25 \times 10^{11}[\text{s}^{-1}](3[\text{cm}])(0.917[\text{g/cm}^3]).$$

Only about 60% of the ionization energy is actually deposited into the target, leading to about 0.33 Watts. Combined with the heat deposit from microwaves (0.5 W) used to dynamically polarize the target, the cooling power of the UVA/JLab evaporation fridge and pumping system is not saturated. However, cooling power is not the only concern. This heat load must be distributed throughout the target so that the target material beads are not over-heated on the material boundary so as to create local depolarization. To do this with electrons a beam rastering system can be used to distribute the beam over the surface of the target face. The slow raster that spirals out is combined with the faster raster system which distributes the beam in a  $2 \text{ mm}^2$  square pattern. The CPS is designed to also utilize the fast raster system – however without also some sort of slow rastering there would be significant depolarization in the region around the photon beam spot due to material interfacial thermal heating (ITH).

The ionizing radiation inside the target is the primary source of the  $\dot{\text{N}}\text{H}_2$  fee radical but also the ITH. Using simulations with the previously mentioned photon flux and a  $2 \text{ mm}^2$  beam profile leads to 25 nA of ionizing radiation at the exit of the target in an area of about  $6 \text{ mm}^2$  (containing 90% of the ionizing particles). Taking this spatial distribution to hold the full 0.33 W heat load from the high intensity photon beam implies that about 100 target beads with an average radius of 1 mm hold all the heat. To calculate the effects of this heat load on the local polarization we must first start with the heat equation for a volumetric heat source. This can be expressed as,

$$C_{p0}T^3\rho\frac{dT}{dt} = \dot{Q} - 3R_\alpha\frac{T^4 - T_B^4}{r_{bead}}. \quad (1)$$

Using the corresponding values, this equation can be solved with the initial condition  $T(0) = 1\text{K}$ .  $\dot{Q}$  is the volumetric heat load per bead which is conservatively estimated to be  $0.72 \text{ W/cm}^3$ . Using the specific heat for  $\text{NH}_3$  of  $C_{p0} = 8.8 \times 10^{-6} \text{ J g}^{-1} \text{ K}^{-4}$ , with ammonia Kapitza resistance  $R_\alpha = 1.43 \times 10^{-2} \text{ W cm}^{-2} \text{ K}^{-4}$ , with  $T_B$  as the liquid helium bath temperature (1 K), and  $T$  is the dynamic material boundary temperature. The solution to this relation gives the boundary temperature as a function of time and is shown in Fig 1.

These results indicates that after a few microseconds the surface of the bead increases by about 0.25 K. We can then estimate the time it takes to heat the bead all the way through from the heat on the surface assuming spatial uniformity,

$$\Delta t = \frac{\rho V C_p \Delta T}{\dot{Q}}. \quad (2)$$

This calculation results in a time of just a few  $\mu\text{s}$  to heat the entire bead from the outer surface. These times are small on the scale of the time it take for the polarization to change. To estimate the time it takes to drive the polarization down from the material beam heating we must consider the DNP rate parameters of  $\text{NH}_3$ . This decay time is related to the microwave power and the spin-lattice relaxation rate. The equations of motion that give the rate of depolarization can be approximated using the form,

$$\frac{dP(t)}{dt} = \beta T^4 (P_{lim} - P(t)). \quad (3)$$

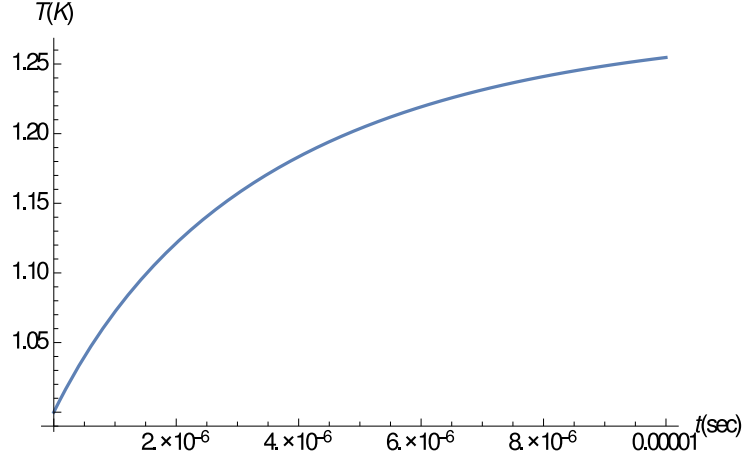


Figure 1. Ammonia bead temperature rise due to the beam heat load.

172 The polarization, limited by the new thermal conditions from Eq. 3, is contained in  $P_{lim}$ ,  
 173 which is an estimate based on the Brillouin function. The parameter  $\beta$  contains the rate  
 174 information and comes from polarization data. The starting polarization of 93% is used  
 175 as an example. Solving Eq. 3 numerically results in an approximation of the polarization  
 176 drop over time.

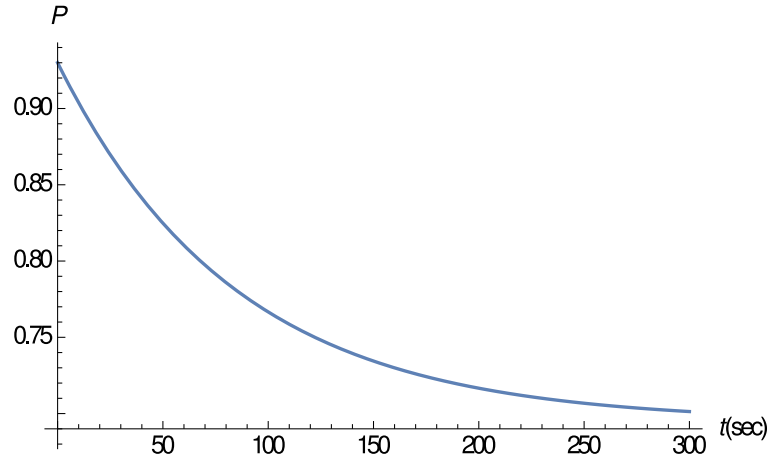


Figure 2. Rotating Target Cup

177

178

179

It is worth noting that calculations here are only estimates and several necessary  
 180 parameters required have considerable uncertainty. We use the results as only a guide  
 181 to give an order of magnitude check on the time need to rotate the target cell. Figure 2  
 182 indicates that the beads should only stay within the same position in the ionizing shower  
 183 for no more than a few seconds or the polarization will decrease. This change would not  
 184 register in the NMR signal. A rotation on the order of once every few seconds is adequate  
 185 for this purpose. The other demand on the target is, of course, the radiation damage  
 186 induced by all forms of scattering in the target. If the dose that is mentioned previously

187 (25 nA) from the ionizing radiation can be distributed over a standard target area of 570  
 188 mm<sup>2</sup>, then the expected depolarization rate from radiation damage is still slower than  
 189 that of an electron beam at 100 nA.

## 190 2 Design of Rotating Target

191 In order to increase the area of the target that the photon beam will interact with a  
 192 rotating target was developed to raster photons over the target cup face, see Fig. 3. The  
 193 Kel-F target cup is machined to include a gear that can be driven from a rotating shaft  
 194 along the target insert. Fig. 3 shows a design of the same dimension of polarized targets  
 195 used in the past (2.5 cm diameter by 3 cm length) that fit within the homogeneous field  
 196 region of the polarizing 5 T magnet. In the design shown there is no additional material

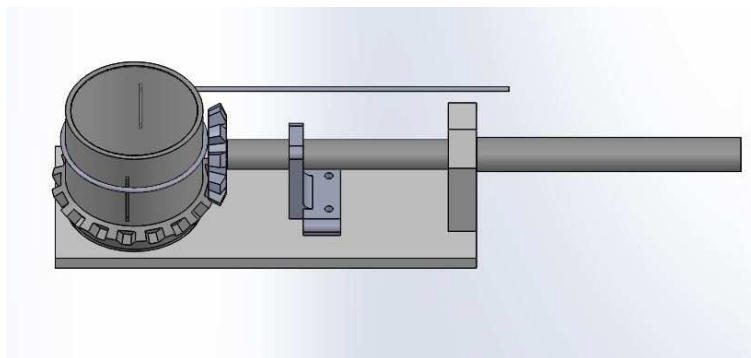


Figure 3. The rotating target cup driven by a gear and shaft with the NMR loop around the  
 197 target cell.

198  
 199 from the cup in the beam-line. The front and back of the target cell are made of a thin  
 200 aluminum foil (not seen in the diagram). The rotation is driven by a gear and shaft. The  
 201 NMR couples inductively to the target material by a coil wound around outside of the  
 202 cup. The rotating shaft passes through the top of the target insert using a vacuum rotary  
 203 feed-through which is then driven by a electric motor.

204 The target rotation in combination with the standard target actuator results in  
 205 an effective slow raster which spirals over the full area of the standard 2.5 cm diameter  
 206 target. The beam collimation provides the spot size on the target and couples directly to  
 207 the resolution characteristics for reconstruction at the cost of holding the beam location  
 208 in space fixed. We can still obtain uniform exposure of the target cell by a combined  
 209 rotation of the target cup synchronized with an up/down movement of the target ladder.  
 210 Rotation of the target cup has already proven viable in many UVA tests. Depolarization  
 211 and homogeneous radiation damage can easily be achieved by continuously moving the  
 212 target at a rate determined by the radius of the circle made through rotation on the target  
 213 surface, spending no more than a few hundred milliseconds on each target location. So  
 214 even near the center only 0.01 Hz is required. To avoid mechanical vibration that can  
 215 induce noise in the NMR signal it is possible to make several rotations in a fixed diameter  
 216 before moving to the next actuator position. This reduces the up and down motion  
 217 required to cover the same area. At UVA rotation rates of several Hz have already been



demonstrated. By completing a fixed number of rotations for each experimental run, false asymmetries and fluctuations from the variations in target bead packing can be averaged out.

### III The Compact Photon Source

#### A Conceptual Design

A traditional source of bremsstrahlung photons includes a radiator, a deflection magnet and focal plane detectors with a large momentum acceptance, and a beam dump for the undeflected electrons. Such a configuration requires significant space along the beam direction and heavy shielding due to the large openings in the magnet and the beam dump. In addition, without tight collimation it leads to a large size of the photon beam at the target due to divergence of the photon beam and the long path from the radiator to the target. The beam spot size contributes to the angular and momentum reconstruction resolution of the resultant reaction products due to uncertainty in the transverse vertex position. Lastly, it often comes with appreciable radiation doses as particles are allowed to propagate over short distances before mitigation of radiation by containment starts to be effective. A new solution for a photon source was proposed in a report at the NPS collaboration meeting in November 2014 about a new experiment for a double polarized wide-angle Compton scattering from the proton (see a detailed analysis of the CPS in Ref. [2]). Reconstruction of the scattered photon in WACS depends on multiple factors including the photon spot size at the target, for which the distance from the radiator to the target is the most important factor. Dedicated studies prepared prior to the WACS proposal submission have shown that a spot size of around 2mm is well matched to preserve the benefits of the proton arm angular resolution and the spatial resolution of the photon arm [3].

The concept of a new source takes advantage of the narrowness of the photon beam relative to the angular distribution of the secondary particles produced in the electron-nuclei shower. Indeed, the photon beam angular spread, dominated by electron multiple scattering in the 10% $X_0$  radiator, is about  $4/E_{beam}[\text{MeV}] \sim 0.4$  mrad, but the secondary particles survived filtering through a one nuclear interaction length ( $\sim 140\text{-}190$  g/cm<sup>2</sup> or  $\sim 15$  cm) of the heavy absorber, have an angular spread of 0.1-1 radian. The main elements of the CPS are shown in Fig. 4. Without loss of photon intensity, a channel (a collimator for the secondary radiation but not for the photon beam) around the photon beam could be as narrow as the photon beam size with natural divergence plus the size of the beam raster. After passing through the radiator, the electron beam should be removed from the photon line by means of a magnet. The length, aperture and field of the magnet are very different in the proposed source from the traditional one. In the traditional source the magnet is needed to direct the electrons to the dump. Because of the large momentum spread of electrons which have interacted in the radiator, the magnet aperture needs to be big and the dump entrance should be even bigger (13% of the beam power would be lost before the beam dump, even with a 10% momentum acceptance of the beam line). In contrast, the proposed source has a dump inside the magnet.



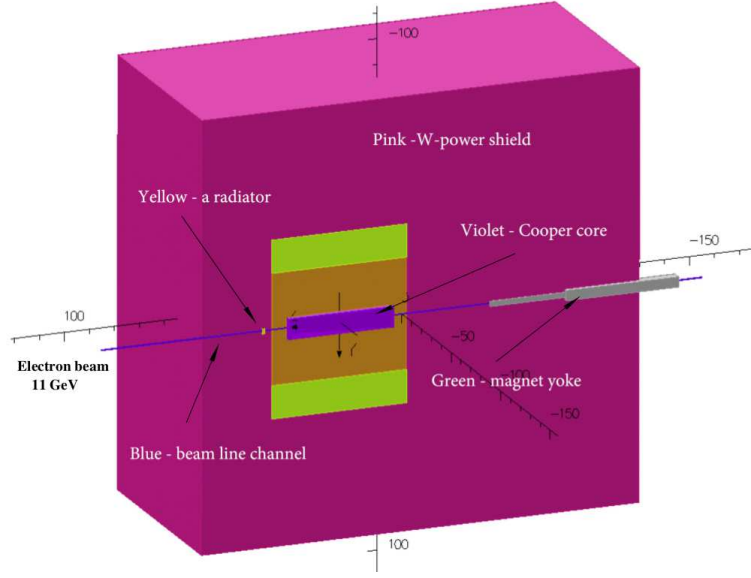


Figure 4. The CPS view.

260 The electron energy dumping starts on the side of the photon beam channel, so a  
 261 shift of the electron trajectory by just 1-3 mm is already sufficient for the start of the  
 262 shower. At the same time, such a deflection needs to be accomplished at a relatively  
 263 short distance (much shorter than the size of the radiation shielding) after the beam  
 264 passes through the radiator to keep the source compact. Indeed, with a deflection radius,  
 265  $R$ , a vertical size of the channel,  $2a$ , and a vertical raster size,  $2b$ , the trajectory enters  
 266 the channel side after traveling in the magnetic field a distance,  $p$ , which varies from  
 267  $p = \sqrt{2R(a-b)}$  to  $p = \sqrt{2R(a+b)}$  (see the scheme in Fig. 5). In the currently

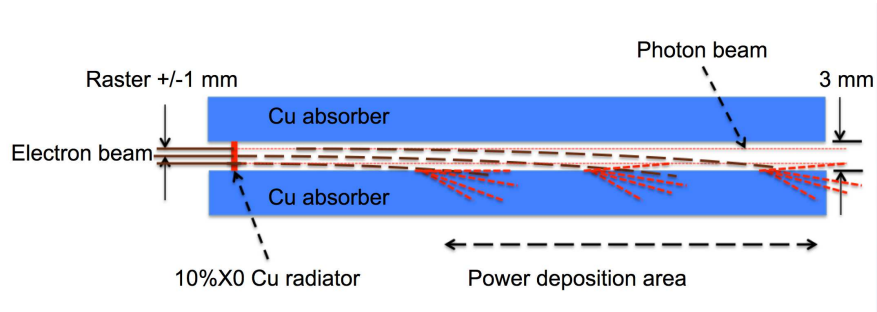


Figure 5. The scheme of beam deflection to the absorber/dump.

268  
 269 proposed CPS magnet the trajectory radius  $R$  is about 10 m for 11 GeV electrons, the  
 270 channel size is 0.3 cm, and the raster size is 0.2 cm, so the distance  $p$  has an average value  
 271 of 17 cm with a spread of 12 cm. A total field integral of 1000 kG-cm is adequate for our  
 272 case, which requires a 50 cm long iron dominated magnet.

273  
 274 The above concept of the combined magnet-dump allows us to reduce dramatically  
 275 the magnet aperture and length, as well as the weight of the radiation shield, due to

the reduction of the radiation leak through the openings and the short length of the source. This consideration opens a practical way forward for the CPS because it leads to a reduction of power deposition density in the copper absorber.

## B Magnet

Normal conducting magnets for high levels of radiation have been constructed at several hadron facilities, including the neutron spallation source at ORNL and the proton complex JPARC. In fact, the radiation level expected in the source allows use of a modest cost kapton tape based insulation of the coils. We designed the magnet with permendur poles tapered in two dimensions, which allows us to reach a strong magnetic field (3.2 Tesla) at the upstream end of the magnet, and moved the coils to 20 cm from the source of radiation. The length of the magnet was selected to be 50 cm and the field integral 1000 kG-cm. Figure 6 shows the longitudinal profile of the magnetic field obtained from OPERA calculations.

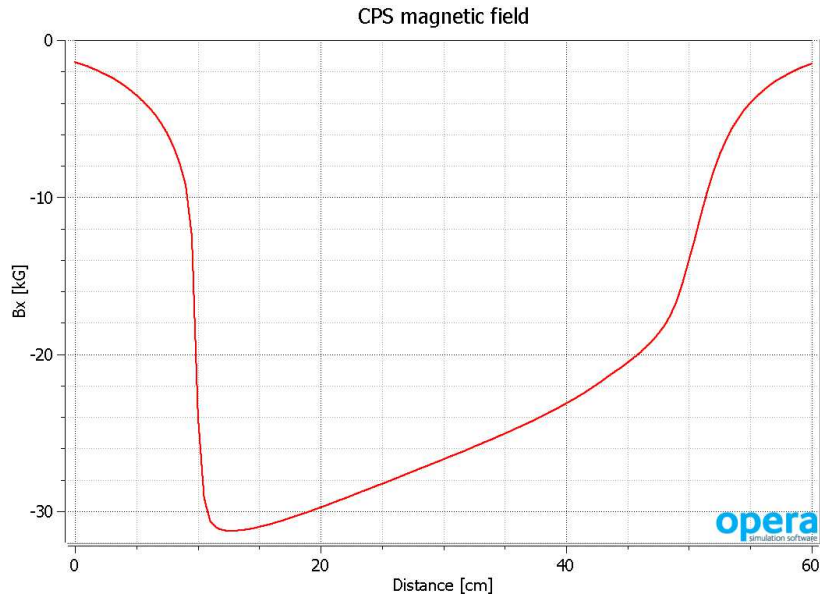


Figure 6. Magnetic field ( $B_x$ ) profile along the beam direction.

## C Central Absorber

The beam absorber will be made of copper, whose high heat conductivity helps to manage the power density. If it is needed, we can use an aluminum absorber, which would help to reduce power density even more by a factor of 2-3 due to a six times larger radiation length, but it would also increase the length of the source length by about 50 cm. The heat removal from the copper absorber is arranged first via heat conductivity to the wider area where water cooling tubes are located. At 10-15 cm from the beam line, the temperature of the copper insert drops to a level below 100°C (the calculation of the energy

deposition was made in both the SIMC and Geant4 frameworks, and the temperature 2-dimensional analysis was performed for the highest power density area). Figure 7 shows the longitudinal profile of the power density according to the MC simulation.

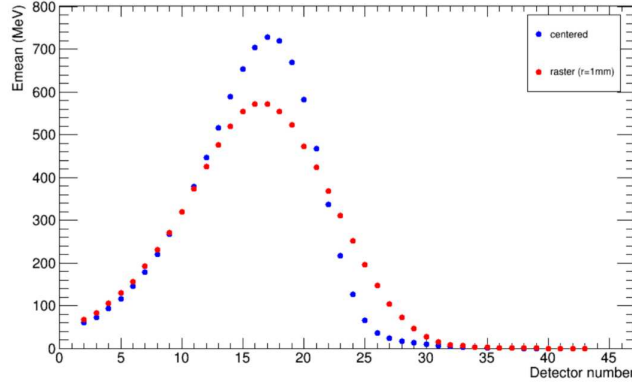


Figure 7. Longitudinal profile of the power distribution (integrated for one cm copper slab) for one 11 GeV incident electron. The maximum power density is at the coordinate 18 cm. The blue dots show the energy deposition for the electron beam centered in a 3 mm by 3 mm channel. The red dots show the same for the beam rastered with a radius of one mm.

The transverse distribution of power is also very important to take into account because, for a high energy incident beam, it has a narrow peak. A detailed MC simulation of power density and 2-dimentional heat flow analysis were performed to evaluate the maximum temperature in the copper absorber. Temperature was found to be below 400°C, which is well in the acceptable range for copper (the calculation was performed for the case of a 11 GeV 30 kW beam and a 10% X0 radiator). Figure 8 shows the temperature profile in the transverse plane at the longitudinal location of maximum power deposition. Cooling of the core will require about four gallons of water per minute at 110 psi pressure (at 30°C temperature rise), which is easy to provide.

## D Tungsten-powder Shield

The amount of material needed for radiation shielding is primarily defined by the neutron attenuation length, which is 30 g/cm<sup>2</sup> for neutrons with energy below 20 MeV and 125 g/cm<sup>2</sup> for high energy neutrons. The neutron production rate by an electron beam in copper is  $1 \times 10^{12}$  per kW of beam power according to a SLAC report (W.P. Swanson, SLAC-PUB 2042, 1977, see Fig. 9). At a distance of 16 meters from the unshielded source for a 30 kW beam, the neutron flux would be  $1 \times 10^7$  n/cm<sup>2</sup>/s, which would produce a radiation level of 110 rem/hr, or 850 times higher than during the RCS experiment at JLab (E99-114) (at a 16-meter distance from the pivot in the upstream direction). A radiation reduction factor of 1000 will be achieved by means of a shield with a mass of 850 g/cm<sup>2</sup>. For the shield outside the magnet, the current design uses tungsten powder, whose high density (16.3 g/cm<sup>3</sup>) helps to reduce the total weight of the device. A thickness of 50 cm was used as a first estimate for the thickness of the outer shield in CPS.

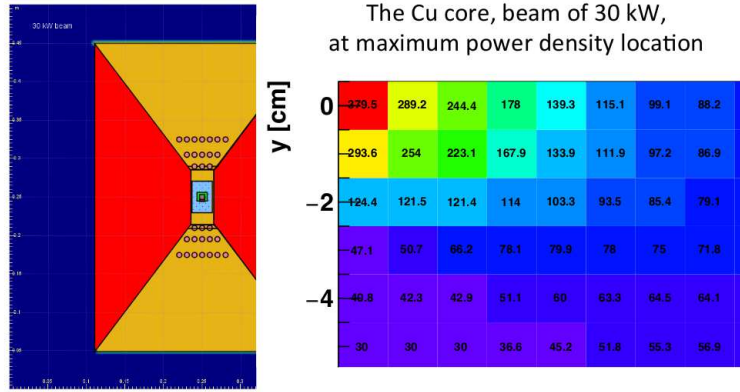


Figure 8. The cross section of the absorber (shown by yellow and blue in the center) with the cooling channels and the temperature map.

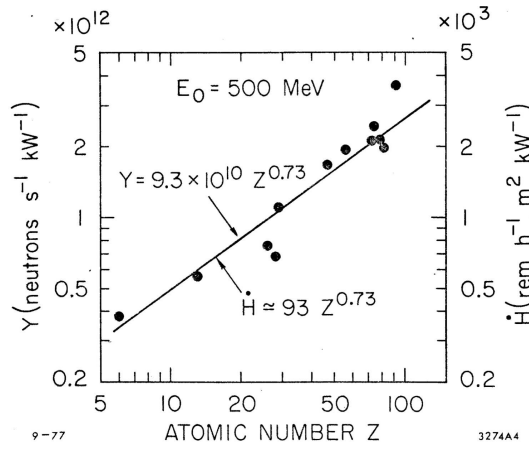


Fig. 12

Figure 9. The neutron yield according to Swanson's report.

## IV Radiation Requirements

The goal of the Compact Photon Source is to convert beam energies of up to 12 GeV with currents of up to  $5 \mu\text{A}$  into a high-intensity source of collimated photons. For the Hall-D adaptation, the  $5 \mu\text{A}$  beam current is limited by the design of the Hall D Tagger Magnet alcove. This corresponds to a 60 kW power limit. For the Halls A/C adaptation, the beam energy is limited to 11 GeV. Many experiments will opt to use the traditional method for photon beam experiments, with the high-current electron beam striking a 10% radiation length Cu radiator. The CPS gain in Halls A/C is foreseen for use with Dynamically Nuclear Polarized targets. Electron beam currents for use with such targets is typically limited to 100 nA or less, to reduce heat loading and radiation damage effects. The equivalent heat load for a pure photon beam impinging such targets

corresponds to a photon flux originating from a  $2.7 \mu\text{A}$  electron beam current striking a 10% Cu radiator. Hence, the CPS design for Halls A/C should be able to absorb 30 kW in total (corresponding to 11 GeV beam energy and  $2.7 \mu\text{A}$  beam current).

In addition, the typical beam time we assume for an approved experiment at JLab is 1000 hours ( $\sim 40$  PAC days). For such a CPS experiment, one needs to fulfill the following radiation requirements:

- Prompt dose rate in hall  $\leq$  several rem/hr at 30 feet from device.
- Prompt dose rate at the site boundary  $\leq 1 \mu\text{rem/hr}$  ( $2.4 \mu\text{rem/hr}$  corresponds to a typical experiment at Jefferson Lab not requiring extra shielding).
- Activation dose outside the device envelope at one foot distance is  $\leq$  several mrem/hr one hour after the end of a 1000 hour run.
- Activation dose at the pivot in the experimental target area, where operational maintenance tasks may be required, is dominated by the dose induced by a pure photon beam, and at one foot distance from the scattering chamber  $\leq$  several mrem/hr one hour after the end of a 1000 hour run (i.e. the additional dose induced by radiation of the main beam absorbed in the CPS is negligible).

The CPS design should combine in a single shielded assembly all elements necessary for the production of the intense photon beam and ensure that the operational radiation dose rates around it are acceptable as outlined in the requirements above. Much of this is achieved by keeping the overall dimensions of the setup limited, by careful choice of materials, and by shielding induced radiation doses as close to the source as possible. Compared to a traditional bremsstrahlung photon source, the proposed solution will present several advantages, including much lower radiation levels, both prompt and post-operational due to the beam line elements radio-activation, as will be shown later.

The CPS conceptual design has been established with extensive and realistic simulations. As validation of the simulation tools used, we have also performed a benchmark comparison using tools such as GEANT3, GEANT4, FLUKA and DINREG. The benchmark results are further described in Appendix 2. After benchmark validation, we have performed an extensive series of radiation calculations to:

- Determine the size and layering of the shielding around the magnet, and the choice of materials (Cu, Cu-W alloy, concrete, borated plastic, etc.).
- Determine the magnet field requirements in terms of peak field, gap size, and field length.
- Determine the radiation level on the magnet coils and based on these results identify radiation hardened materials that might be used in building the coils.
- Determine the radiation level on the polarized target electronics.
- Determine the radiation level immediately next to the device as well as at the experimental hall boundary.

376 The logic behind the CPS hermetic shielding design is that radiation ( $\gamma$ ,  $n$ ) from the  
 377 source should be a few times less than from a photon beam interacting with the material  
 378 of a polarized target. The CPS is designed to meet the radiation level requirements  
 379 specified in Appendix 2 for an electron beam current of  $2.7\mu\text{A}$  (30 kW), run time of 1000  
 380 hours, and the photon source as close to the target as possible. The shielding design  
 381 consists of tungsten powder and 10 cm of 30% borated plastic. The addition of the latter  
 382 has considerable impact in reducing the neutron flux escaping the CPS, illustrated in  
 383 Figure 13.

## 384 V Radiation Studies and Shielding Design

385 In this section we will describe several different configurations for comparison, the  
 386 first of which is the default situation for dynamically nuclear polarized targets in Hall C  
 387 and elsewhere, which is that of a 100 nA incident electron beam. The second configuration  
 388 corresponds to the equivalent photon flux created by a  $2.7\mu\text{A}$  electron beam on a 10%  
 389 Cu radiator incident on the same polarized target system. In this scenario, we remove  
 390 all the secondary particles generated in order that it mimics a pure and background-free  
 391 photon beam. The third scenario is one with the CPS under the same conditions, a  $2.7\mu\text{A}$   
 392 electron beam on a 10% Cu radiator, for which all the radiation background is included  
 393 in the simulation. In some cases we have simulated only the effect of the CPS, while in  
 394 others the CPS and the target system combined are considered.

### 395 A Prompt Radiation Dose without a Target

396 In order to help introduce the shielding concept of the CPS, we start by comparing  
 397 the prompt radiation doses as calculated in a ring detector covering a radial range between  
 398 5 and 10 cm from the beam line. We first calculate the prompt dose originating from  
 399 a  $2.7\mu\text{A}$  electron beam hitting a 10% Cu radiator a distance of 2.15 m upstream of  
 400 the pivot. There is no target system in this simulation, which means that all prompt  
 401 radiation originates from the interaction between the primary beam and the radiator.  
 402 Figure 10 shows two-dimensional dose rates originating from photons only (top left),  
 403 from neutrons only (top right), from all particles (bottom left), and the one-dimensional  
 404 prompt radiation dose along the beam direction (bottom right). Obviously, except for the  
 405 neutron contribution most of the prompt radiation is created along the beam direction.  
 406 The prompt radiation levels reach roughly 40 rem/hr, of which only around 200 mrem/hr  
 407 is in the form of gamma radiation and 10 mrem/hr from neutrons. The remaining and  
 408 clearly dominant contribution are the charged electrons and positrons created, inducing  
 409 further showers.

410 A striking difference is observed in the case of a  $2.7\mu\text{A}$  electron beam incident on  
 411 a 10% Cu radiator as before, but now located within the CPS. Figure 11 illustrates the  
 412 prompt radiation dose along the beam direction. The y-axis scale on this figure is the  
 413 same as in Figure 10 (bottom right panel). One can therefore clearly see that the prompt  
 414 radiation (again, in a 5 to 10 cm ring detector along the beam axis) within the CPS  
 415 is much higher (300 times, because with CPS the full power of the beam is deposited).



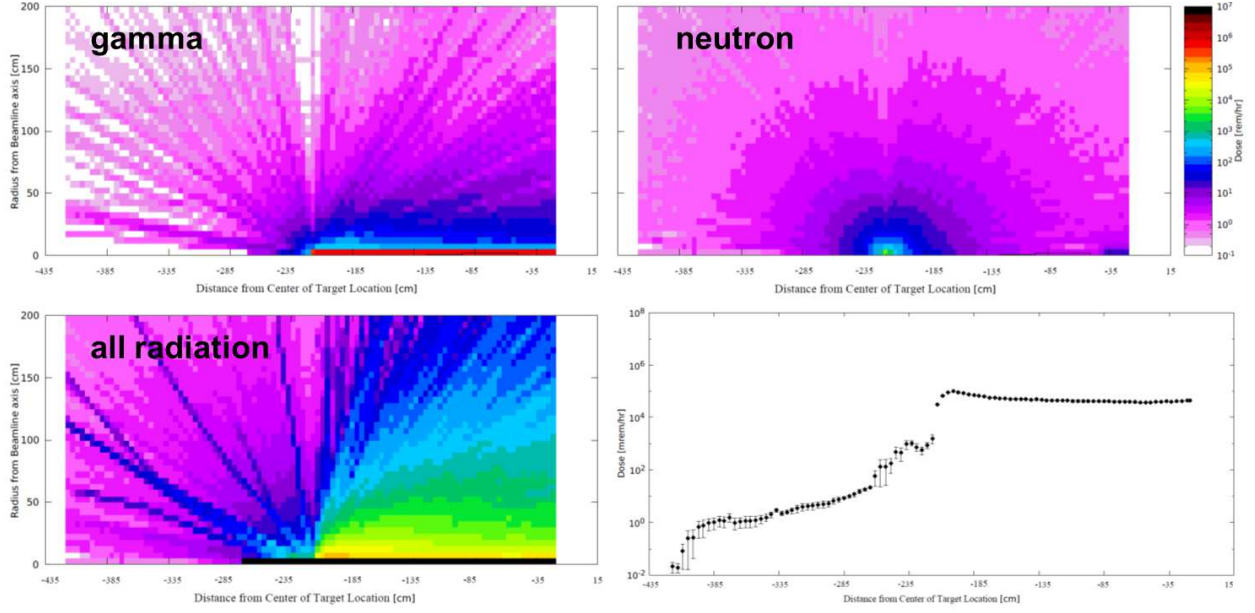


Figure 10. Two-dimensional dose rates as originating from photons only (top left), from neutrons only (top right), from all particles (bottom left) and the (one-dimensional) prompt radiation dose along the beam direction (bottom right).

Crucially, however, the prompt radiation dose outside the CPS is reduced by a factor of over 1000 to roughly 15 mrem/hr. This factor is entirely consistent with the reduction factor of estimated previously in section III D.

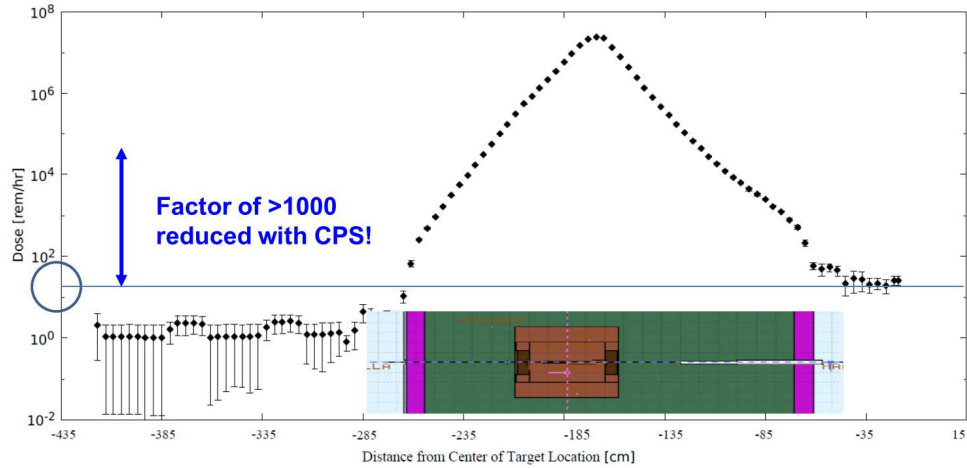


Figure 11. Two-dimensional dose rates as originating from photons only (top left), from neutrons only (top right), from all particles (bottom left) and the (one-dimensional) prompt radiation dose along the beam direction (bottom right).

This extremely important result is further illustrated in Figure 12. In stark contrast with the case without the CPS, there is now no contribution to the prompt dose from photons, electrons and positrons – the neutron-only dose rate is nearly identical to the



all-radiation rate. The fourth panel in Figure 12 (bottom right) illustrates how well an optimized CPS shielding concept absorbs the prompt radiation. Outside the CPS the prompt radiation dose rate on the surface (indicated by the outer black rectangular lines) is reduced to a maximum level of roughly 10 rem/hr. This shielding concept is so effective because of the fact that the development of showers generated by interactions of the primary beam is highly suppressed and the resultant secondary particles contained. This confirms that with a CPS the following requirement can be met: **prompt dose rate in hall  $\leq$  several rem/hr at 30 feet from device.**

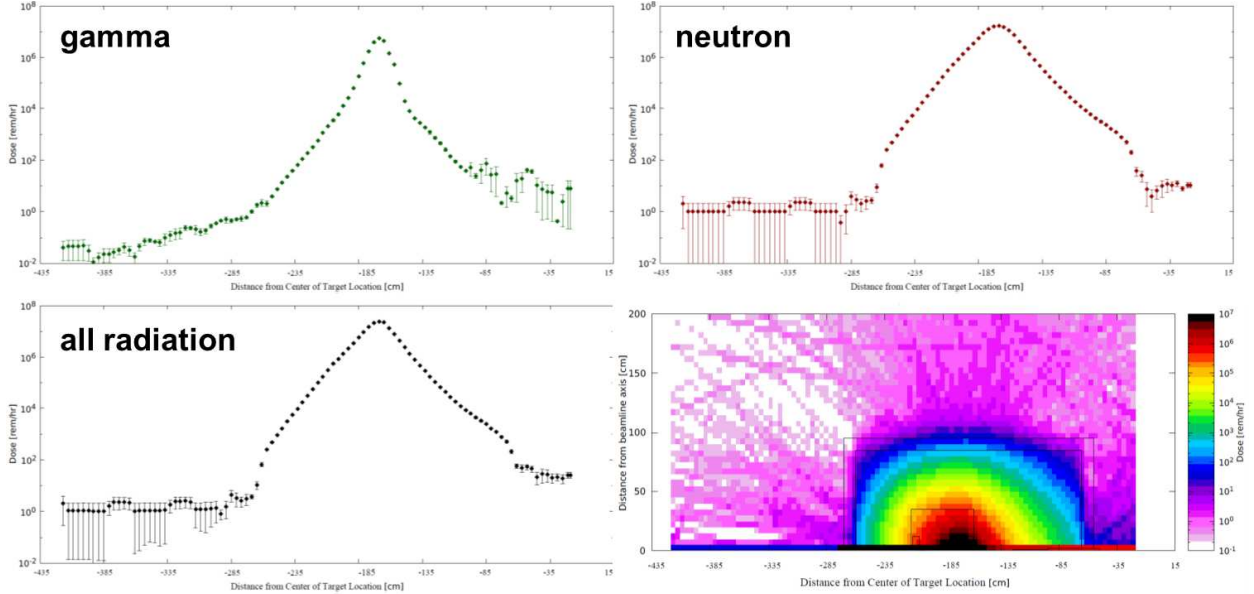


Figure 12. The (one-dimensional) prompt radiation rates as originating from photons only (top left), from neutrons only (top right), and from all radiation sources (bottom left). The fourth panel (bottom right) illustrates how well an optimized CPS shielding concept absorbs the prompt radiation, outside the CPS the prompt radiation is on the surface (indicated by the outer black rectangular lines) already reduced to a level of roughly 10 rem/hour at most.

## B Impact of Boron and Shielding Optimization

It is well-known that the neutron flux through a surface can be drastically reduced by the addition of boron as a result of the very high capture cross section of  $^{10}\text{B}$ . We simulated this effect by calculating the neutron flux at the CPS boundary assuming various thicknesses of tungsten shielding (65, 75 and 85 cm radial), and then adding 10 cm of borated (30%) plastic. The result can be seen in Figure 13, which shows the neutron flux as function of neutron energy (on a logarithmic scale). Adding 10 cm of tungsten clearly reduces the neutron flux as expected, but a much more drastic reduction is seen when the 10 cm of borated plastic is added. Thus, in our design we assume an outer layer of 10 cm-thick borated plastic for the CPS. In order to demonstrate how well the shielding design has been optimized, Figure 14 shows a comparison between the prompt radiation dose

441 rates with the optimized shielding design (right) and with 10 cm less tungsten shielding  
 442 and no borated plastic (left). (Note that in these panels the CPS magnet is assumed to  
 443 be at the center of the beam line, in contrast with earlier figures.)

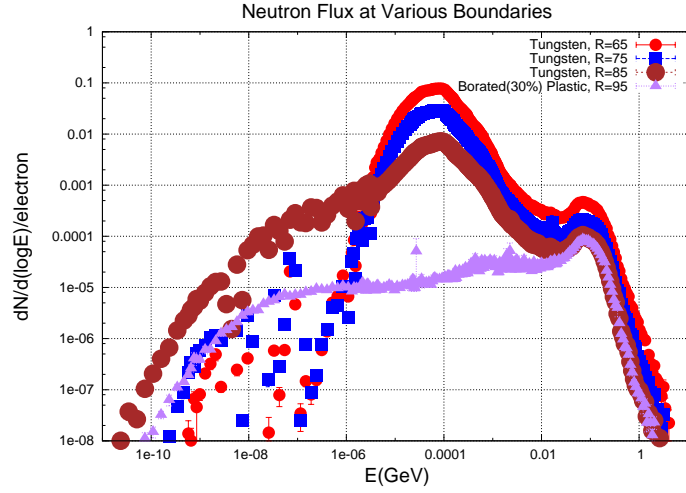


Figure 13. Impact of boron on shielding properties.

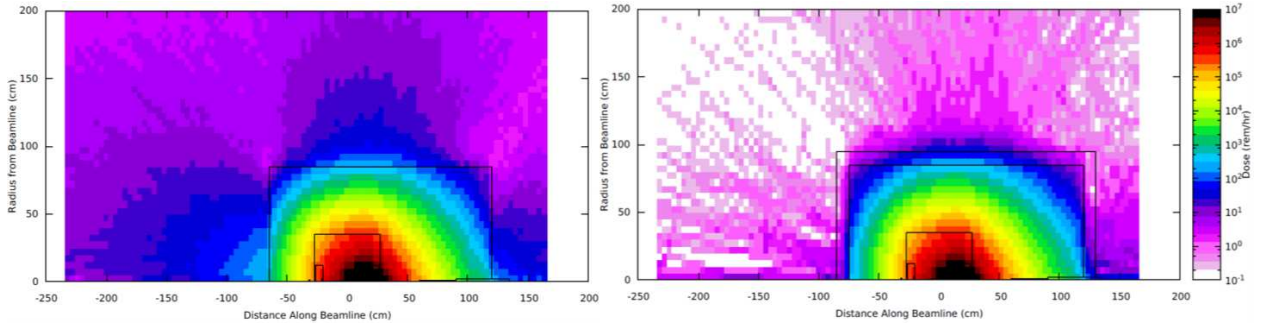


Figure 14. The prompt radiation rates with the optimized shielding design, whereas in the left panel we show the same prompt radiation rates without extra shielding (10 cm less of tungsten shielding, and no borated plastic). Note: these are with the CPS magnet centered around "zero" along the beam line.

## 444 C Prompt Dose Rates at the Boundary

445 In benchmark calculations assuming spheres of pure shielding materials (see a more  
 446 extensive description of the benchmark calculations in Appendix 2 we find that the prompt  
 447 dose rate estimates at the RBM-3 boundary are  $0.24 \mu\text{rem/hr}$  for a 3 meter diameter iron  
 448 sphere and  $2.4 \mu\text{rem/hr}$  for a 1.5 meter diameter tungsten sphere. The baseline design  
 449 for CPS shielding is assumed to be 85 cm thick tungsten surrounded by 10 cm of borated  
 450 plastic. Hence, the boundary dose is **below the  $2.4 \mu\text{rem/hr}$  that corresponds to a**

451 **typical experimental run at Jefferson Lab, for which additional local shielding**  
452 **is not required.** If required, further reductions in the boundary dose can be achieved by  
453 optimizing the baseline design in terms of material choice and geometry. Note also that  
454 for Hall D, the CPS design is compatible with the site boundary limits as the standard  
455 Hall D tagger magnet can dump up to 60 kW in a local beam dump. Indeed, the Hall D  
456 tagger building has been designed assuming a 12 GeV electron beam up to a current of  
457 5  $\mu$ A. For the CPS, one can thus assume the Hall D tagger magnet building shielding is  
458 appropriate in the case for up to 60 kW being dumped in the CPS itself, albeit with the  
459 possibility that additional local shielding may be required.

## 460 D Activation Dose without a Target

461 We now turn to the activation dose expected around the CPS following beam-on  
462 conditions. Figure 15 shows the calculated activation dose one hour after a 1000-hour  
463 experiment has been completed with the same conditions as before (2.7  $\mu$ A, 10% Cu  
464 radiator, with shielded CPS). The radiation calculations show the activation dose outside  
465 the CPS is reduced to the order of roughly 1 mrem/hr. To quantify this further, Figure 16  
466 shows the activation dose radially away from the CPS. The activation dose outside the  
467 CPS is reduced to 2 mrem/hr at the surface and reduces radially outward. At one-foot  
468 distance, it is reduced to about 1.5 mrem/hr, while at two-feet distance it is further  
469 reduced to less than 1 mrem/hr. Hence, this demonstrates that the current design meets  
470 the requirement that **activation dose outside the device envelope at one foot**  
471 **distance is  $\leq$  several mrem/h after one hour following the end of a 1000 hour**  
472 **run.**

473 Note that these estimates do not depend much on the assumed 1000-hour continuous  
474 running assumption, as similar dose rates are seen in a calculation for a 100-hour contin-  
475 uous run, reflecting that much of the activation is instant. Furthermore, activation dose  
476 rates do not drop appreciably after one hour or even one day. On the other hand, after  
477 one month the activation dose rates at the CPS surface will be reduced by up to a factor  
478 of ten. Inside the CPS the activation dose rate can be up to 1 krem/hr, which is why the  
479 CPS will be moved laterally to the side after an experiment rather than disassembled.

## 480 E Radiation Dose Rates with a Target

481 In building further on our radiation calculations, we have included the polarized  
482 target scattering chamber and target system. In Figure 17 we illustrate our setup and  
483 show a side-view of the CPS, indicating the magnet, the tungsten-powder shield, the layer  
484 of borated plastic, and also the scattering chamber with polarized target system. The  
485 description of the scattering chamber and polarized target includes: the exact diameter of  
486 the scattering chamber and all the ports with accurate dimensions and window materials;  
487 and the polarized target material including the liquid helium surrounding the target beads.

488 Figure 18 is included here for completeness. It illustrates the 1-MeV neutron equiv-  
489 alent damage to silicon (in neutrons/cm<sup>2</sup>), which is the relevant quantity to quantify the  
490 risk of radiation damage to sensitive electronics. The result, not surprisingly, shows that

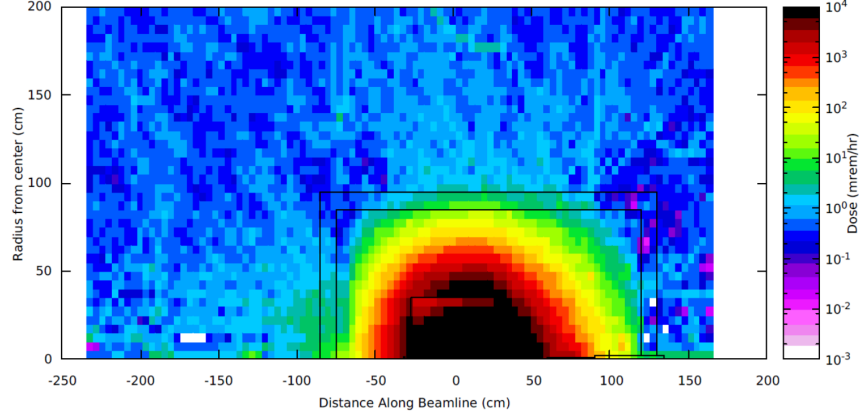


Figure 15. Calculated activation dose one hour after a 1000-hour experiment under the described conditions ( $2.7 \mu\text{A}$ , 10% Cu radiator, with shielded CPS) has been completed. Note: these are with the CPS magnet centered around "zero" along the beam line.

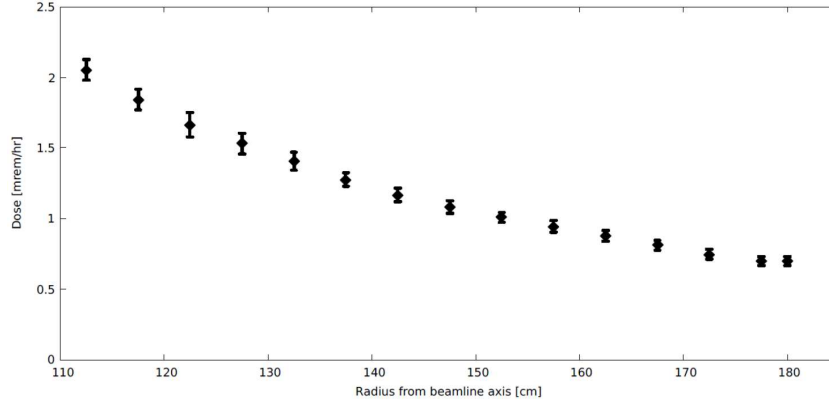


Figure 16. Activation dose outside CPS 1 hour after a 1000 hour run is 2 mr/hr on contact and reduced radially outwards.

there is a narrow cone in the forward direction, along the beam axis, up to roughly one meter, in which sensitive electronics should not be placed if at all possible.

Figure 19 shows the prompt dose at the target for different configurations. The distance  $R$  is radial distance from the pivot, with the radius of the scattering chamber boundary at 50 cm. The various colors on the figure represent the various types of configurations studied: the  $100 \text{ nA}$  electron beam (red downward triangles), the  $2.7 \mu\text{A}$  photon beam (blue upward triangles), the CPS without polarized target (black circles), and the CPS with polarized target (mauve squares). At the boundary of the scattering chamber in the  $100 \text{ nA}$  electron beam configuration, the default operating mode for polarized beam experiments with dynamically nuclear polarized targets in Hall C to date, the prompt dose is roughly 1 rem/hr. In the  $2.7 \mu\text{A}$  photon beam scenario it is roughly 30 rem/hr, which simply reflects the fact that even if a  $2.7 \mu\text{A}$  pure photon beam deposits the same heat load in a target as a  $100 \text{ nA}$  electron beam, the radiation rate is much higher. The CPS with polarized target scenario is identical to the pure photon beam case, further

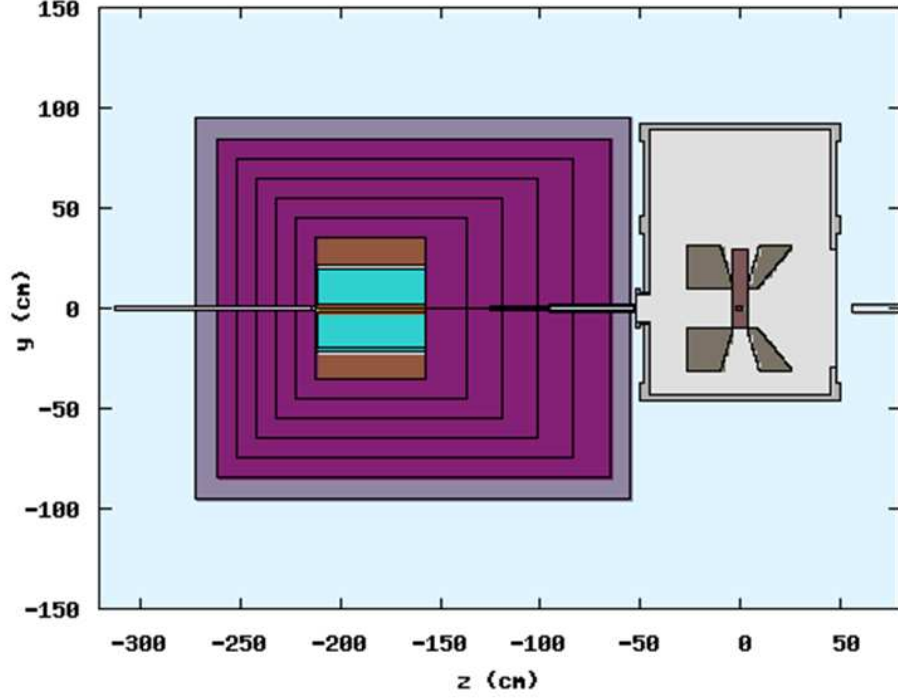


Figure 17. Side view of the Compact Photon Source, indicating the magnet, the W powder shield, and the layer of borated plastic, and also the scattering chamber with polarized target system.

demonstrating that no additional radiation comes from the CPS.

Figure 20 is perhaps more instructive, in that it shows the activation dose rates for the same three configurations. The vertical size of the figure panels have been adjusted such that equal dose rates line up from left to right. One directly can see therefore that the  $2.7 \mu\text{A}$  *photon beam* configuration has a much higher activation dose rate than the  $100 \text{ nA}$  *electron beam* case. This again reflects what was seen in the previous figure for the prompt radiation dose rate, as there are many more photons coming from a  $2.7 \mu\text{A}$  electron beam on a 10% Cu radiator than there are from a 100 nA electron beam on a roughly 3% dynamically nuclear polarized target. More interestingly, the effect of the CPS is again negligible: activation near the target does not come from the CPS itself, but rather from the photon beam we have created. The price to pay is that one ends up with a roughly constant 0.1 mrem/hr activation level at large radial distances, but this is manageable.

We also indicate in the various panels of Figure 20 how quickly the activation rates drop (after one hour, one day, one week, and one month). One can see that much of the 0.1 mrem/hr activation level induced by the deployment of the CPS has decayed away after a week. This is consistent with what was observed in the example of the activation levels at radial distances around the CPS above.

Lastly, we illustrate in Figure 21 in a two-dimensional plot the activation dose rates one hour after a 1000 hour run with the CPS, a  $2.7 \mu\text{A}$ , 11 GeV beam on a 10% radiator and the polarized target system (at  $z = 0$ ). The 1 mrem/hour contour is indicated. This

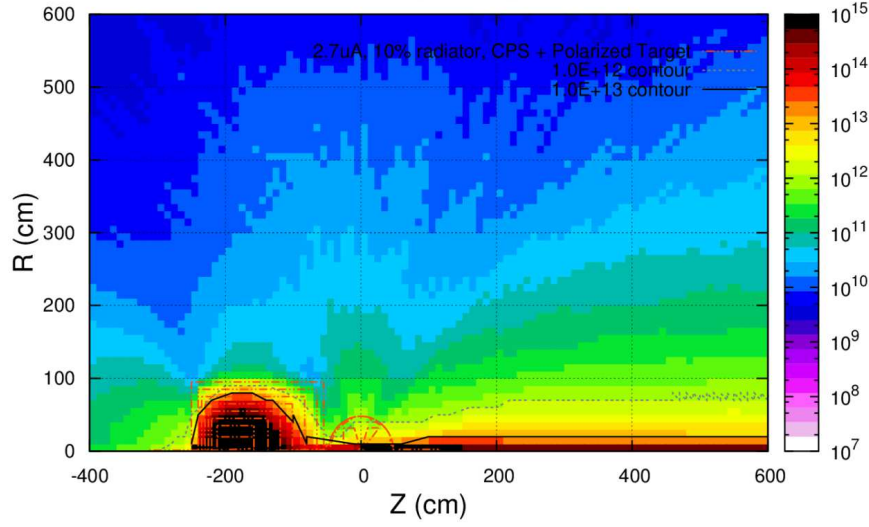


Figure 18. 1-MeV neutron equivalent damage to silicon (in neutrons/cm<sup>2</sup>).

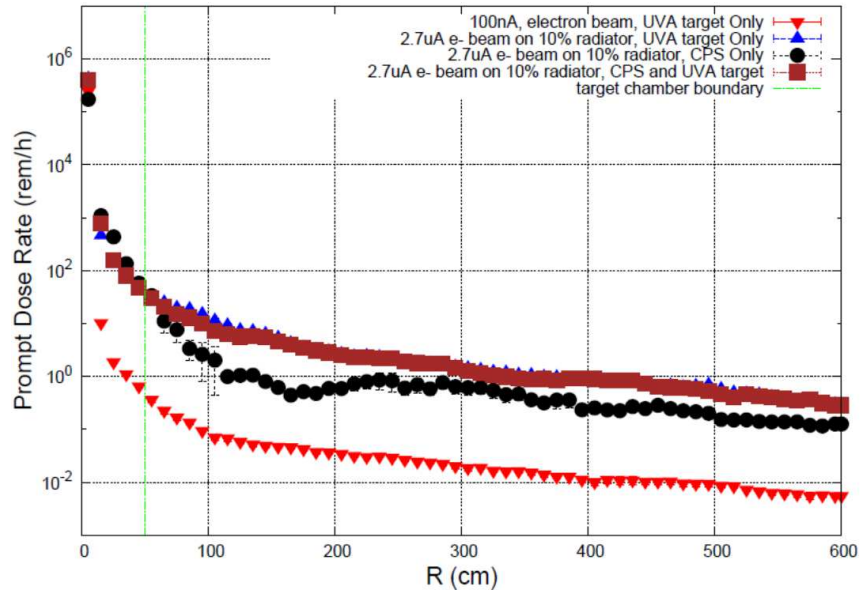


Figure 19. Prompt dose at the target for different configurations. Distance R is radial distance from the pivot, with the radius of the scattering chamber boundary at 50 cm.

526 demonstrates that with the current CPS baseline design, the **activation dose at the**  
 527 **pivot in the experimental target area, where operational maintenance tasks**  
 528 **may be required, is dominated by the dose induced by a pure photon beam**  
 529 **and is at one-foot distance from the scattering chamber  $\leq$  several mrem/hr**  
 530 **one hour after a 1000 hour run, and also that the additional dose induced by**  
 531 **radiation of the main beam absorbed in the CPS is negligible.** These were the  
 532 last of the radiation requirements that were introduced in section IV.



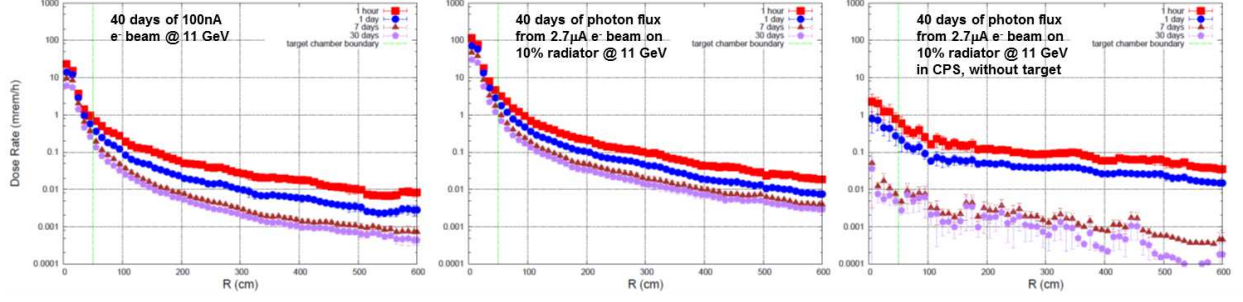


Figure 20. Activation dose rates at the target for different configurations. Distance  $R$  is radial distance from the pivot, with the radius of the scattering chamber boundary at 50 cm.

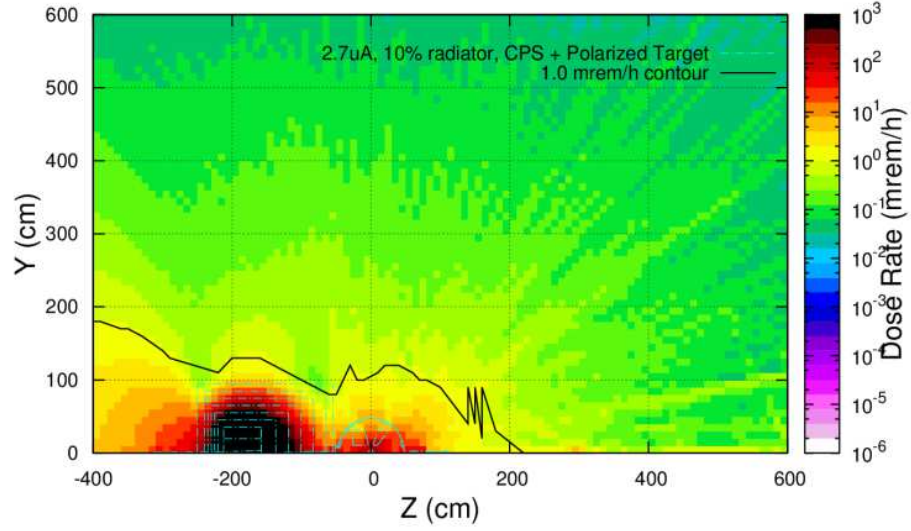


Figure 21. Activation dose rates one hour after a 1000 hour run with the Compact Photon Source, a  $2.7 \mu\text{A}$  beam and a 10% radiator, at 11 GeV beam energy, and the polarized target system (at  $z = 0$ ). The 1 mr/hr contour is indicated.

## 533 VI Engineering and Safety Aspects

534 In this section we will describe the engineering and safety aspects of the CPS.  
 535 We will start with a summary of material considerations taking into account the high  
 536 radiation and power inside the CPS, folding in further insights of the radiation studies as  
 537 relevant for materials for the CPS and the dynamically nuclear polarized target. Then  
 538 we describe various engineering aspects such as cooling and magnetic forces, and further  
 539 considerations for assembly and installation of the CPS. We will also outline safety aspects  
 540 related to the CPS, such as interlocks and fast raster operation during CPS experiments,  
 541 and post-experiment removal. Lastly, we will give a cost estimate.



## 542 A Material Considerations

543 The level of radiation of the CPS experiments is well below what is typical for many  
 544 high-luminosity experiments in Halls A and C using regular cryogenics target systems  
 545 and/or radiators. The prompt radiation level on the polarized target is higher than  
 546 before, which is simply an artefact of the higher photon flux associated with the higher  
 547 figure-of-merit of the CPS experiments. The radiation level on the polarized target coils,  
 548 due to the interaction of the photon beam with the polarized target material, amounts to  
 549 about 500 rem/hr as illustrated in Fig. 22.

550 The radiation levels in the CPS magnet coils, at a distance of 20 cm from the  
 551 radiation source, are reduced to below 1 Mrem/hr (see e.g. Fig. 12, bottom right), and  
 552 allow the use of a modest-cost Kapton tape-based insulation of the coils [5].

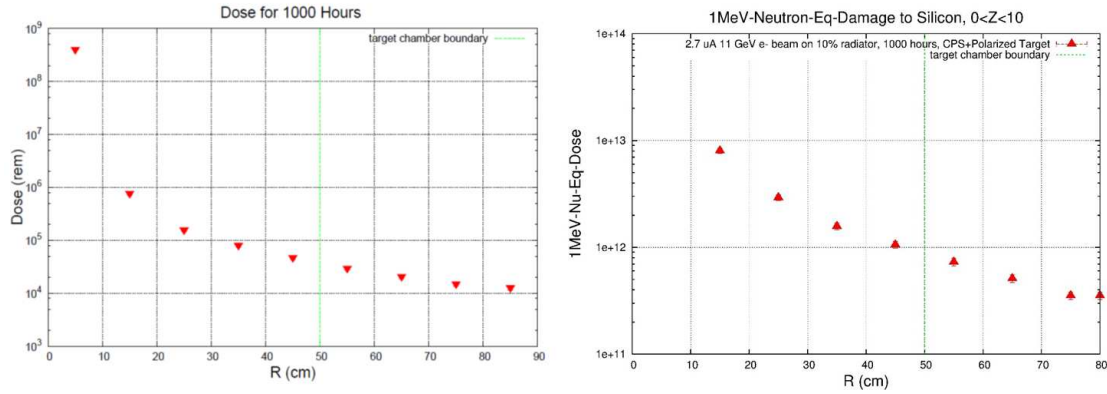


Figure 22. The prompt dose rates (right) and the resulting 1 MeV neutron equivalent damage to silicon (left) in the target area, assuming a 1000 hour run with the Compact Photon Source with a 2.7 mA beam, a 10% Cu radiator, and 11 GeV beam energy. The polarized target system is at  $z = 0$  and the nominal target chamber radius is 50 cm. The target coils are at about 20 cm from the beam line. The dose for 1000 hours of beam time at the target coils is 5 times  $10^5$  rem and the 1 MeV neutron equivalent damage is 5 times  $10^{12}$  neutrons/cm<sup>2</sup>. The contribution of the CPS backgrounds to these numbers is negligible (contributing 2.5% only).

553 As described in Section III B, we explicitly added a small insert of copper within the  
 554 tungsten-powder shielding of CPS to act as the beam power absorber. The combination  
 555 of a small  $\pm 1$  mm vertical raster and the magnet field shaping spreads the beam power  
 556 density over a large surface, such that the temperature of the copper absorber was less  
 557 than 400°C. This is well below its melting temperature of 1,085°C.

## 558 B Cooling and Magnetic Forces

559 Cooling of the core requires 4 gallons per minute at 110 psi pressure. This will  
 560 result in a 30°C temperature rise of the cooling water. These values are consistent with  
 561 provisions in Hall C. Activation of the cooling water of the CPS magnet and beam dump  
 562 is likely and a closed-cycle cooling system is planned. Hall C has had secondary in-Hall

water-cooled dumps of comparable power before, for polarized target experiments in the 6-GeV era. High-power radiators are also not new and have been used with tens of  $\mu\text{A}$  on 10% radiation length targets, also with closed-loop water cooling systems. The magnet heat and dump heat can be removed through a heat exchanger to either the Hall C air or LCW. Any activation of the CPS will be confined to a very small volume and in the event of a leak external contamination will be minimized. A leak pan under the CPS could easily be included to catch and confine any leakage up to and including a total loss of primary coolant. A modular pallet mounted design would be efficient and would include primary coolant pumps, DI resin beds, heat exchanger, surge tank, controls, and instrumentation and manifolds.

The CPS magnet will be located relatively close to the 5 Tesla solenoid of the polarized target whose mutual forces need to be taken into account in the design of the support structure and may require compensation. Preliminary analysis was already performed in the technical note in 2015 for iron-based shielding. In the design the iron-based shielding is replaced by the more effective tungsten-powder shielding, which also much reduced the forces. Residual fields and forces from the CPS magnet will require iron shielding to avoid interference with the Polarized Target magnet.

Another magnetic consideration is the effect on field quality at the polarized target. The fields and gradients imposed on the polarized target will not be large but they must be compensated at the  $10^{-4}$  level. Some further magneto-static effort to model the target environment and design a compensation system is required.

## C Assembly and Installation Plan

The CPS should be completely pre-assembled before installation. The pre-assembly can be done in the Hall or more likely in the Test Lab High Bay, or equivalent area. The outer dimension of the CPS tungsten-powder shielding as outlined for optimized shielding (see Fig. 14, right panel) is 1.7 m by 1.7 m by 1.95 m, or a volume of  $5.63 \text{ m}^3$ . From this, one needs to subtract the inner box including the magnet, which amounts to  $0.26 \text{ m}^3$ . This means a net volume of  $5.37 \text{ m}^3$ , or 88 tons, for the optimized tungsten-powder shielding presented. In total, the CPS weight is estimated to be 100 tons. Hence, a reinforced floor is required for CPS assembly, as exists in both the Test Lab High Bay and the Hall itself. Note that if one would reduce the overall size of the W-powder shielding by 5 cm on each side, it would imply an increase of the radiation levels by about 50%, and a reduction to  $4.48 \text{ m}^3$  or 73 tons (for the W-powder). If one would remove an additional 10 cm only on the bottom side, towards the floor, for an additional factor of two increase in radiation level in the direction of the floor, this reduces to 68 tons.

During assembly and after completion the CPS can be measured and fiducialized to facilitate final alignment in Hall C. Progressive measurement and fiducialization will eliminate problems with position references becoming hidden. Transporting the CPS to (or within) Hall C in one piece will preserve the alignment and avoids introduction of errors due to dis-assembly and re-assembly. This would require a large crane in Hall C, similar as for examples was used for G0 installation and removal, and for SOS removal.

The CPS will be installed in the area upstream of the Hall C pivot (see Fig. 23). The polarized target chamber will be installed instead of the regular scattering chamber, and

606 the CPS will be installed replacing the final Hall C beam line girder and one horizontal  
 607 bend magnet, the most downstream magnet of the 12-GeV Hall C beam line. The final  
 608 Hall C beam line girder (Fig. 24) contains the beam position diagnostics for the regular  
 609 Hall C electron scattering experiments, including a double set of superharp and beam  
 610 position monitoring systems. These are used to define the incident beam position and  
 611 beam angle, but not needed for the CPS experiments (where we rather need to know the  
 612 beam position on the radiator). The horizontal bend magnet, the most downstream (blue)  
 613 magnet on Fig. 25 was installed as precaution to prevent beam steering of the SHMS at  
 614 small angles. This magnet is not required, especially as the foreseen CPS experiments  
 615 used ancillary detector systems such as NPS and BigBite. Instead of this magnet, a small  
 616 girder with one beam position monitor and superharp system is foreseen, to define the  
 617 electron beam-radiator interaction point.

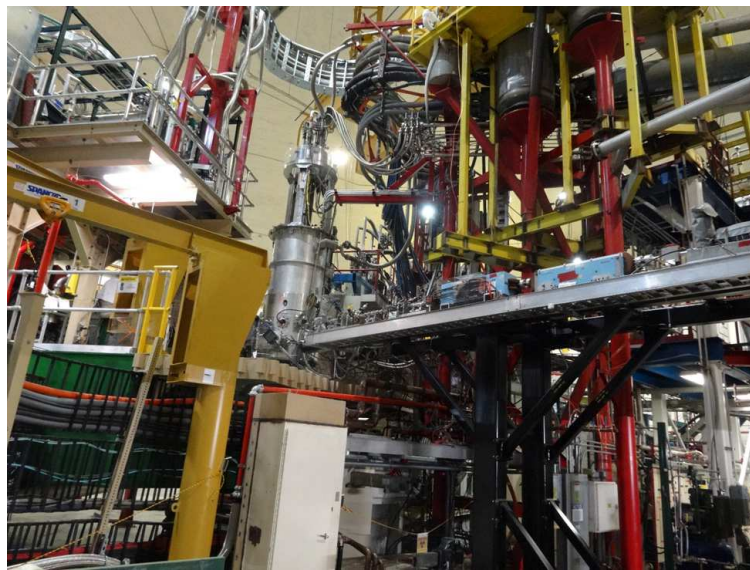


Figure 23. Final Hall C girder, SHMS data cable conduits and environment.

618 The downstream portion of the last beam line girder is cantilevered over the SHMS  
 619 data cable hoses which arc around the pivot and permit rotation. The SHMS cable  
 620 conduits cannot be removed or significantly modified. They do permit legs for the CPS  
 621 stand, but they may limit the rotation of the SHMS somewhat. A platform for the  
 622 CPS could perhaps be welded and bolted from the top of the pivot cylinder (under the  
 623 scattering chambers) to an upstream stand. The addition of CPS stands and/or a welded  
 624 platform still requires further design and engineering. We do note that one support leg  
 625 of a platform (the lowest yellow support bar on Figs. 23 and Fig. 25) will need to be  
 626 moved, but this can be done.

627 Installation in Hall C will consist of the following steps:

- 628 • Removal of the final beam line girder
- 629 • Removal of the horizontal bend magnet
- 630 • Presurvey and mount of CPS stand to Hall C floor

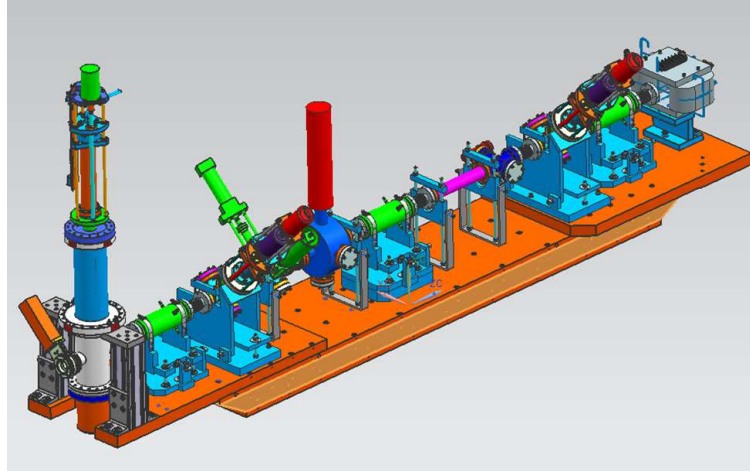


Figure 24. The present final girder in Hall C.



Figure 25. Closer view on final Hall C girder.

- 631 • Transport and crane in complete CPS using a larger than 100 ton truck crane
- 632 • Survey and alignment of CPS
- 633 • Installation of new small beam girder and instrumentation (upstream of CPS)
- 634 • Survey and alignment of new girder
- 635 • Connect CPS magnet power and water and test
- 636 • Connect new girder and test
- 637 • Restore beam vacuum in Hall C
- 638 • CPS hot checkout



## 639 D Equipment Safety and Interlocks

640 Whereas the closed-loop cooling requirements of the CPS in themselves are not  
641 new to Hall C, the combination of a high-power radiator, magnet and beam dump in-  
642 side a shielded box impose reliability and remote handling considerations. The primary  
643 engineering controls providing personnel protection are to make the design as robust as  
644 possible, with large safety margins, and evade disassembly for maintenance and repair, or  
645 equipment removal, altogether.

646 The CPS should be heavily instrumented for early detection of problems such as low  
647 coolant flow, leaks, low pressure, high temperature, and high conductivity. The protection  
648 and safety of the CPS begins with the design which must err on the side of conservatism  
649 especially in the magnet coil design and dump cooling. A low current density design  
650 is envisioned, not to exceed 500 Amps/cm<sup>2</sup>. Individual coil pancakes leads should be  
651 extended to an area outside of the magnet and shielding for easy access. There should  
652 be NO electrical or coolant joints inside the CPS shielding. Every separate sub coil of  
653 the CPS magnet should have thermometry, klixons and flow measurements to avoid any  
654 possibility that one of the separate current paths can overheat due to lack of sufficient  
655 coolant, a leak or a bad electrical joint. Voltage monitoring of each sub coil should insure  
656 against overheating from any source including internal blockage, leaks, flow restrictions or  
657 bad electrical connections. Extra insulation between sub coils and between the coil and  
658 ground should be added to prevent ground faults. Lastly, a commercial power supply is  
659 assumed and these come with a wide array of internal interlock protections. The available  
660 interlocks and signals would be fed into the FSD system.

661 To protect equipment during CPS operations, a dual protection scheme is suggested  
662 using both the Hall C BPM system and direct instrumentation of the fast raster magnet  
663 itself. The BCMs would monitor beam position and motion in close to real time and  
664 coil voltage monitoring on the raster coils would provide ample early warning of raster  
665 problems. Both these independent signals would be fed into the FSD system. Radiator  
666 temperature could be monitored to provide a third independent protection system, and if  
667 implemented, thermocouples mounted on the radiator should be robust against radiation  
668 damage and provide fast enough protection against radiator overheating.

669 Simulations of various magnet failure modes such as reduced or no water flow,  
670 overheating, etc., can be used to proof test instrumentation and interlocks. These tests  
671 would be performed in Hall C after final installation as part of the usual hot checkout  
672 procedures.

## 673 E Post-Experiment Removal Plan

674 The CPS is expected to become activated and contaminated by the completion of  
675 the experiment. Activation levels inside the CPS are expected to be and remain high,  
676 until well after experiment completion. Exposure to Hall C staff will be minimized by  
677 designing the CPS for a one-piece removal. The total weight of the CPS is about 100  
678 tons, too heavy for the Hall C crane so this will require use of a large truck crane. The  
679 CPS will then be stored on the periphery inside Hall C, most likely at the location where  
680 the beam either enters or exits the Hall boundary, under the beam line. This eliminates

681 the need for staff to dis-assemble the CPS.

682 Water disconnects using self-sealing connectors can be used to eliminate any primary  
683 cooling water loss. The DC Power supply and air-cooled cables will be disconnected and  
684 removed as they are not expected to be activated. The cooling water pumps, controls,  
685 DI resin beds and heat exchanger will likely have contaminated water inside but will not  
686 otherwise be activated. The cooling pallet can be removed to storage intact or the water  
687 drained and stored separately or disposed of. The radiator infrastructure can be stored  
688 as with other Hall C experiments using radiators.

689 After the CPS removal, the small girder removal, and the CPS stand removal, the  
690 regular last beam line girder and horizontal pre-bend magnet can be installed and surveyed  
691 in their locations again, to restore the default 12-GeV Hall C electron beam line.

## 692 **F Initial Cost Analysis**

693 A preliminary cost analysis has been made. The W-powder and magnet costs are  
694 based on a vendor quotation and estimate, other items are engineering estimates. The  
695 CPS cost will be dominated by the cost of W-powder. Here, we assumed the cost for the  
696 optimized shielding design, requiring 88 tons. We could reduce with roughly 20% but this  
697 would increase radiation levels by up to a factor of two.

- 698 • Tungsten powder shield, 88 tons - \$3300K
- 699 • CPS Magnet, includes mechanical design and tooling - \$98K
- 700 • Cu core absorber and closed loop water cooler - \$25K
- 701 • WCu (20%) insert, 1 ton - \$100K
- 702 • Borated plastic outer layer - \$100K
- 703 • Support structure and elevation jacks - \$50K
- 704 • Beam line: Radiator system and raster magnet with power supply - \$50K
- 705 • Beam line: small girder with superharp and BPM - \$50K
- 706 • Closed-loop magnet and dump cooling system -\$25K
- 707 • Instrumentation, controls, and interlocks - \$50K
- 708 • Rented crane and crew - \$10K/day

709 The total cost estimate amounts to nearly \$4M, with the tungsten-powder as the dominant  
710 part. The reduction of tungsten powder can act as contingency. Alternatively, one could  
711 use surplus lead as a cheaper shielding material option, but it would roughly double the  
712 CPS weight.

## VII Acknowledgements

We thank Paul Brindza for helpful discussions and providing valuable input for the writing of this document.

- 
- [1] D. Keller, “The UVa approved and proposed experiments”, in arXiv:1704.00816.  
[2] B. Wojtsekhowski and G. Niculescu, “Conceptual Design Report, A Compact Photon Source”, Supplementary material for the WACS proposal PR12-15-003 to the JLab PAC 43, June 2015; in arXiv:1704.00816.  
[3] D. Hamilton, “Photon Beam Requirements for Wide-Angle Compton Scattering”, in arXiv:1704.00816.  
[4] P.K. Kloeppel, “Design for 25-kW beam dumps at 100 MeV and 500 MeV”, CEBAF-TN-90-205; M. Wiseman, C.K. Sinclair, R. Whitney, M. Zarecky, “High Power Electron Beam Dumps at CEBAF”.  
[5] V.V. Petrov, Yu.A. Pupkov, a report “BINP TESTING OF RADIATION RESISTANCE OF THE MATERIALS USED FOR PRODUCTION OF ACCELERATOR MAGNETIC SYSTEMS”, Novosibirsk, 2011

## Appendix 1: Concept Transfer to Hall D

The intense photon source is one component of the  $K_L$  beam. The experimental method can be summarized as follows: electrons hit a copper radiator, the resulting photons hit a Be target, and a beam to  $K_L$  is produced. The search for missing hyperons is a strong motivation for this setup.

The new setup utilizes the Hall D Tagger vault, properly shielded by design to accomodate the medium power beam dump capable of accepting up to 60 kW of 12 GeV electron beam, assuming that proper local shielding is set around the dump. The presently installed dump is placed behind the iron labyrinth walls, and is surrounded by a massive iron shielding, made of iron blocks available at the time of construction. The standard GlueX setup is optimized for operations using very thin radiators producing relatively low intensity photon beam such that the beam electrons losing energy to photon production in the radiator may be detected and counted in the tagger hodoscope counters. The present setup is not suitable for production of massively more intense photon beams needed for the  $K_L$  production, due to the expected overwhelming radiation and activation levels in the vault.

The CPS will be located downstream of the tagger magnet. The tagger alcove has more space than that available in Hall A/C, so positioning and shielding placement are simpler. Indeed, the CPS implementation in Hall D may have a different length and magnet field, as well as shielding. A total floor loading of the implementation up to 100t is acceptable. If one uses a 2nd raster system for Hall D to compensate for the initial 1mm raster, this can be an equivalent essential design to the Hall C/A one.

As discussed in section IV, the Compact Photon Source converts beam energies of up



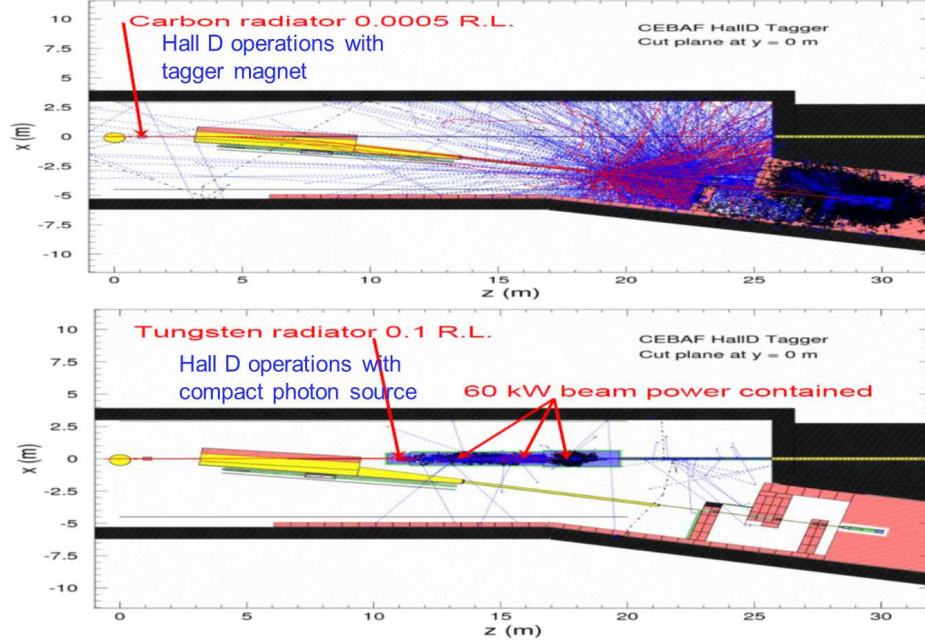


Figure 26. 2D projection of backgrounds in the Hall D alcove for both, the nominal GlueX beam/dump and the  $5\mu\text{A}/\text{CPS}$  configuration.

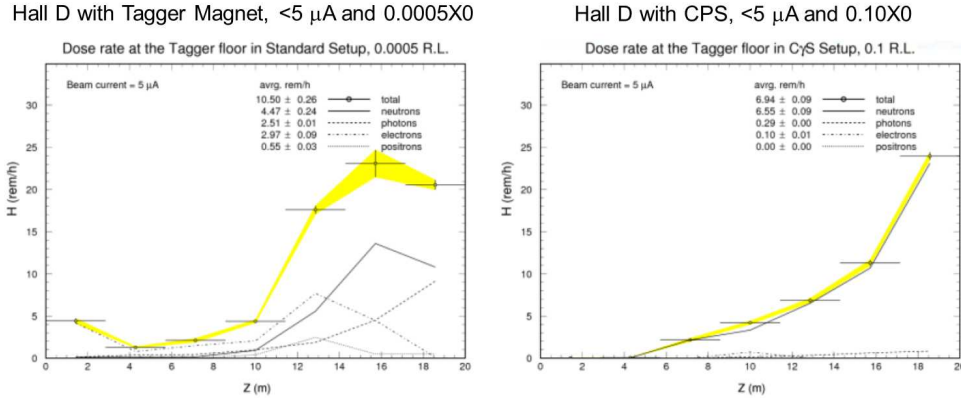


Figure 27. Dose rate at the tagger in standard configuration (left) and with CPS and 10% radiator (right). The CPS with its optimized shielding design does not increase radiation levels beyond standard configuration.

752 to 12 GeV with currents of up to  $5\mu\text{A}$  into a high-intensity source of collimated photons.  
 753 For the Hall-D adaptation, the  $5\mu\text{A}$  beam current is limited by the design of the Hall D  
 754 Tagger Magnet alcove. This corresponds to a 60 kW power limit. Note that the ceiling  
 755 shielding of the Tagger hall above the CPS position is the same as it is above the existing  
 756 60 kW dump. No radiation increase at the site boundary is thus expected with respect to  
 757 60 kW operations using the existing dump. Figs. 26 and Fig. 27 illustrate how the CPS  
 758 stops the electron beam and absorbs almost all beam energy inside, and therefore provides  
 759 excellent shielding. Running the CPS at full beam power produces radiation fields in the

760 Hall D tagger area, comparable with running regular Hall D experiment utilizing a very  
761 thin radiator in front of the tagger magnet.

## 762 Appendix 2: Benchmark comparison

763 From the engineering standpoint, two of the most important aspects in the design  
764 and subsequent building of a Compact Photon Source are the ability to properly shield the  
765 radiation produced inside the source and to dissipate the resulting heat in a safe manner.  
766 While the latter point was addressed earlier in this document, in this Appendix we focus  
767 on the former issue, specifically detailing the steps taken to benchmark the simulations  
768 used in assessing the prompt, as well as the residual (activation) radiation level around  
769 the CPS and in the experimental Hall. Even though they have been mentioned before, it  
770 is worth reiterating the basic radiation level constraints associated with experiments at  
771 JLab:

772 From the radiological protection point of view the following set of limitations should  
773 be satisfied, conservatively assuming typical expected experimental run conditions:

- 774 • Beam energy: 11.5 GeV Beam electron beam
- 775 • Current:  $2.6 \mu A$
- 776 • Beam Power (based on the above) = 30 kW
- 777 • Run time:  $\sim 1000$  hours

778 For the typical, high current JLab experiment the radiation dose rate parameters  
779 must stay within the following limits:

- 780 • Dose rates in the Hall should be under several  $rem/h$  at 10 m from the device
- 781 • Dose rates at the boundary should be under  $1 \mu rem/h$  during the run
- 782 • Dose rates outside the device envelope at a foot distance from the device should be  
783 under several  $mrem/h$  after one hour following the end of the 1000 hour run

784 In order to gain an understanding of the radiation levels likely to be produced by  
785 the CPS and to ultimately design the optimal shielding for it, one relies on Monte Carlo  
786 simulations and over the years the nuclear and particle physics community<sup>1</sup> has developed  
787 a series of very sophisticated simulation programs. In time these programs became more  
788 complex, with several physical processes that can be turned on and off, various thresholds  
789 and cutoffs that might greatly influence the result yet they are buried deep inside the code.  
790 Therefore, one has to be careful in using and interpreting the results of such simulations  
791 because, as suggested above, the same simulation can give vastly (i.e. orders of magnitude  
792 differences) different results with only (seemingly) minor changes in the input parameters.

793 Ideally one would want to **ground-truth** the simulation by **experimentally mea-**  
794 **suring** a small but relevant setup and verify that the simulation results agree with the

---

<sup>1</sup> As well as related areas such as nuclear medicine, astronomy, defense, etc.

795 measured radiation levels of that setup. For the current study this step was not done  
 796 explicitly, though one can argue that one of the simulation programs used (Geant3) was  
 797 extensively **ground-thruth-ed** as the JLab RadCon group compares the radiation levels  
 798 measured at boundary of the experimental Halls with the Geant3 predictions.

799 To benchmark the simulations used in the CPS design a couple of relatively simple  
 800 radiation scenarios were independently simulated using three different simulation pro-  
 801 grams (Geant3<sup>2</sup>, Fluka<sup>3</sup>, and Geant4<sup>4</sup>) by the three groups involved in this process, as  
 802 follows:

- 803 • JLab group (led by P.D.): used Geant3
- 804 • UVa group (led by J.Z.): used Fluka
- 805 • JMU group (led by G.N.): used both Geant4 and Fluka

806 The geometry that was simulated was a simple sphere with a small cylindrical hole  
 807 bored in it such that the 30 kW, 11.5 GeV beam interacts inside the sphere (at  $z = 30$  cm  
 808 for the Fe sphere and at  $z = -15$  cm for the W sphere).

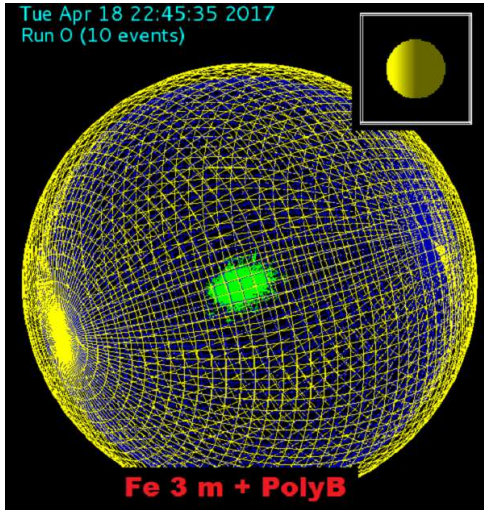


Figure 28. Fe sphere with the Borated Poly layer, as simulated in Geant 4.

Four of these setups were simulated:

- A 300 cm diameter **Fe** sphere
- A 150 cm diameter **W** sphere
- A 300 cm diameter **Fe** sphere with an outer 10 cm Borated Polyethylene layer (5 % Boron by weight)
- A 150 cm diameter **W** sphere with an outer 10 cm Borated Poly layer

The results of these parallel simulations are summarized in the Table below.

809 Examining these results one notes the reasonable agreement between the Geant3  
 810 and Geant4 simulation, though factors of 1–2 could not be ruled out in the differences  
 811 (and are to be expected in these types of estimations). The radiation levels predicted for  
 812 these spheres leads one to conclude that the optimization of the CPS shielding satisfying  
 813 the safety requirements in the Halls and outside ought to be possible. The addition of a  
 814 borated polyethylene layer seems to be absolutely critical in moderating and absorbing  
 815 low energy neutrons. This becomes very important if one choses<sup>5</sup> Fe as (part of) the  
 816 shielding material.  
 817  
 818

<sup>2</sup> The only code currently setup for calculating the radiation at the JLab boundary is Geant3.

<sup>3</sup> Fluka is the only choice for activation calculations.

<sup>4</sup> The development of the Fortran-based Geant3 code has ceased long time ago and the community has/is migrating toward the C++ based Geant4.

<sup>5</sup> For example for cost containment.

	Dose Rates [mrem/h]								
	JLab DINREG/Geant3			JMU Geant4			UVa Fluka		
	n	$\gamma$	total	n	$\gamma$	total	n	$\gamma$	total
3 m Fe	146	0.44	146.44	123.2	0.56	123.76	10	0.039	10.039
3 m Fe + Poly- B	0.8	2.8	3.6	0.284	0.56	0.844	0.11	0.063	0.173
1.5 m W	13	0.06	13.1	6.34	0.33	6.67	1.7	0.0002	1.7002
1.5 m W+Poly-B	2.7	0.003	2.7	1.76	1.28	3.04	0.15	0.0007	0.1507

Table I. Geant3, Fluka, and Geant4 prompt radiation comparison for Fe and W spheres.

One notes that a dose rate of  $\sim 2.4 \mu\text{rem}/h$  at the boundary correspond to a "regular" normal experiment, not requiring extra shielding measures, corresponding to about the "200% of allowable design boundary dose rate" (that is, the dose rate at which the dose accumulation would be 10 mrem if such conditions are run for a half of the calendar year continuously).

The Fluka simulation (carried out in parallel at UVa and at JMU) was able to provide residual radiation (due to activation) at various time intervals: 1 hour, 24 hours, 7 days, 30 days. Sample results for the 3 m Fe sphere, one hour after the end of the irradiation cycle (assumed to be 1000 hours of 11.5 GeV, 2.6  $\mu A$  beam) are shown in the Figures below.

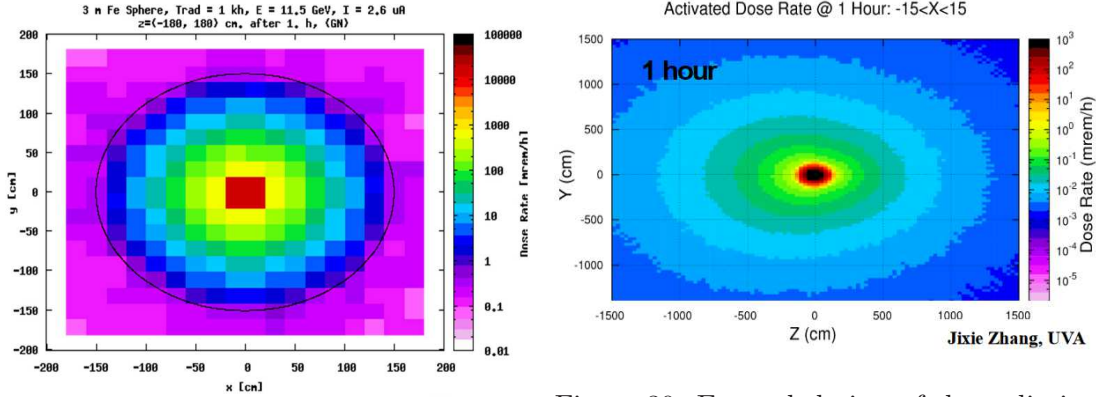


Figure 29. Radiation level one hour after the end of the irradiation period. Closeup view of the JMU Fluka result.

Figure 30. Expanded view of the radiation level one hour after the end of the irradiation period (UVa Fluka result). Both plots correspond to the 3 m Fe sphere.